Adsorption (2012) 18:469–482
DOI 10.1007/s10450-012-9434-y

Optimal flushing flow rates in para-xylene simulated moving-bed considering geometric factor of dead volume

Young-Il Lim

Received: 16 May 2012 / Accepted: 26 September 2012 / Published online: 11 October 2012

Abstract The complex geometry of dead volume is often modeled into a simplified geometry, but little attention has been paid to how the simplified geometry of dead volume influences one-dimensional (1D) SMB modeling. This study investigated effects of the geometric factor of dead volume on 7-zone para-xylene (PX) simulated moving-bed (SMB). This work demonstrated that a complex geometry of dead volume can be modeled into a simple geometry by using a geometric factor in the 1D SMB simulations. Optimal flushing flow rates of the PX SMB were found by the parametric study on recovery and purity, employing the geometric factor to a simplified geometry.

Keywords Simulated moving-bed (SMB) · Para-xylene (PX) · Dead volume · Geometric factor · Axial dispersion; flushing

Nomenclature

Notation

a	numerator parameter of Langmuir isotherms
b	denominator parameter of Langmuir isotherms
BH	bed-head as a dead volume
BL	bed-line as a dead volume
BT	bed-tail as a dead volume
C	fluid concentration (kg/m^3)
$\bar{C}$	time-averaged concentration (kg/m^3)
C_D	desorbent concentration (kg/m^3)
C_F	feed concentration (kg/m^3)
C_{in}	inlet concentration (kg/m^3)
C_{SFi}	second flush inlet concentration (kg/m^3)
CSTR	Continous Stirred Tank Reactor
D_{ax}	axial dispersion coefficient inside adsorptive bed (m^2/min)
$D_{ax,dead}$	axial dispersion coefficient inside dead volume (m^2/min)
d_{BH}	bed-head diameter (m)
d_{BL}	bed-line diameter (m)
d_{BT}	bed-tail diameter (m)
d_c	column diameter (m)
d_{dead}	dead volume diameter (m)
EB	ethylbenzene
k	overall mass transfer coefficient (min^{-1})
L_{BH}	length of bed-head (m)
L_{BL}	length of bed-line (m)
L_{BT}	length of bed-tail (m)
L_c	bed length (m)
L_{dead}	dead volume length (m)
L_{diff}	axial dispersion intensity factor (m)
$L_{diff,dead}$	axial dispersion intensity factor inside dead volume (m)
LDF	linear driving force
LF	line flushing
MX	meta-xylene
N	bed number
N_{CFL}	CFL number
N_{mesh}	number of mesh points
N_{time}	number of time steps
N_{shift}	number of shiftings
OX	ortho-xylene
PDE	partial differential equation
PDEB	para-diethylbenzene
Pe	Peclet number ($= v_L L_c / D_{ax}$)
Pe_{dead}	Peclet number inside dead volume ($= v_{dead} L_{dead} / D_{ax,dead}$)

Y.-I. Lim (✉)
RCCT, FACS, Department of Chemical Engineering,
Hankyong National University, Anseong 456-749, South Korea
e-mail: limyi@hknu.ac.kr

PX	para-xylene
Q_D	desorbent flow rate (m^3/min)
Q_E	extract flow rate (m^3/min)
Q_F	feed flow rate (m^3/min)
Q_{LFi}	line flush inlet flow rate (m^3/min)
Q_{LFo}	line flush outlet flow rate (m^3/min)
Q_R	raffinate flow rate (m^3/min)
$Q_{recycle}$	recycle flow rate (m^3/min)
Q_{SFi}	secondary flush inlet flow rate (m^3/min)
Re	Reynold number ($= d v_L \rho/\mu$)
SF_i	secondary flushing inlet
SMB	simulated moving-bed
t	time (min)
TMB	true moving-bed
V_{BL}	volume of bed-line (m^3)
V_c	column volume (m^3)
V_{dead}	dead volume (m^3)
v_{dead}	velocity inside dead volume (m/min)
v_L	interstitial velocity inside the adsorptive bed (m/min)
x	dimensionless variable of axial distance
z	axial distance (m)

Greek letters

ε_b	bed voidage
θ	dimensionless variable of time
μ	liquid viscosity (kg/m/s)
ρ	liquid density (kg/m^3)
ρ_p	apparent particle density (kg/m^3)
τ	shifting time (min)

1 Introduction

Para-xylene (PX) is the most widely used xylene isomer in the petrochemical industries with a 6 % average annual growth rate for the next decade (Minceva and Rodrigues 2002; Stern et al. 2008). Nowadays, about 60 % of PX worldwide is produced by PX simulated moving-bed (SMB) technology (Minceva and Rodrigues 2007), which offers the advantages of a high driving force, resulting in low solvent consumption, small apparatus size, low investment cost, and high yield (Azevedo 2001; Lim et al. 2010). SMB is a continuous counter-current multicolumn chromatographic process, which has been successfully commercialized in petrochemicals, sugars, pharmaceuticals, bio-molecules, and chiral separations (Antos and Seidel-Morgenstern 2001; Bosma 2001; Juza et al. 2000; Sá Gomes et al. 2009; Seidel-Morgenstern et al. 2008; Wooley et al. 1998). This technology was developed by UOP in the 1960s to overcome the solid circulation problem in true moving-bed (TMB) concept (Broughton and Gerhold 1961), using a flow scheme that simulates a continuous counter-current flow of adsorbent without actually moving it (Minceva and Rodrigues 2005; Pais et al. 1998). The flow scheme is achieved by holding adsorbent as the stationary phase while periodically moving the introduction and withdrawal ports of liquids simultaneously to one column ahead (Grosfils 2009). The ports divide the fixed beds of SMB into several zones. Conventional SMB is divided into 4 zones by the inlet ports (desorbent and feed) and the outlet ports (extract and raffinate).

In industrial- or pilot-scale SMB, dead volumes inflict a significant influence on practical operations (Grosfils et al. 2010; Katsuo et al. 2009; Lim et al. 2010; Minceva and Rodrigues 2003). Dead volumes are always present due to the tubes (lines), valves, pumps, and column beds which may account for up to 3 % of the unit volume in SMB plants (Jin and Wankat 2007; Azevedo et al. 1998). Particularly for the PX SMB configuration, each tube (or bed-line) connecting a rotary valve to adsorbent beds is shared for the introduction and withdrawal of process streams. Hence, the bed-line would be contaminated by the residue of the other stream in the previous shifting unless an appropriate action is taken (Minceva and Rodrigues 2003). To overcome this problem, the PX SMB unit applies internal and external flushing sequences added to conventional four-zone SMB port shifting, which increases the total number of SMB zones to seven or eight (Broughton and Gerhold 1961; Frey 2007; Lim et al. 2010; Minceva and Rodrigues 2003; Noe 1999; Wei 1998). With the intensive and practical applications of SMB, a complex mathematical model considering dead volumes and bed-line flushing becomes a crucial issue in this field.

Grosfils et al. classified the dead volumes into moving and fixed parts (Grosfils 2009; Grosfils et al. 2010). The extra-column dead volumes located at before and after an adsorptive column (bed-head and bed-tail, respectively) were considered to be a part of the moving dead volume, whereas the bed-line connecting the inlet and outlet streams to an adsorptive column was assorted as the fixed dead volume. Several studies have addressed the effects of extra-column and bed-line dead volumes, as well as the flushing of dead volume on SMB performance. A simple way to treat the extra-column dead volume was to use an effective bed length and bed voidage (Beste et al. 2000). A theoretical analysis of the extra-column dead volume in terms of the time delay was reported in both the triangle theory framework (Katsuo et al. 2009; Migliorini et al. 1999) and the standing wave design (Mun et al. 2003). The dynamics of extra-column dead volume was represented by a convection-diffusion model without adsorption (Jin and Wankat 2007; Katsuo et al. 2009; Zabka et al. 2008). The discontinuous feature of concentrations was represented by distinguishing three different stages like time events during one switching period, when the fluid trapped inside the bed-line dead volume is flushed out (Minceva and Rodrigues

2003). A comprehensive dynamic SMB model including both extra-column and bed-line dead volumes in a 7- and 8-zone PX SMB was developed incorporating an extended node model (Lim and Bhatia 2011; Lim et al. 2010).

The dead volume and its representative diameter are normally measured experimentally, and an actual complex geometry is modeled as a simplified geometry having the same dead volume. However, little attention has been paid to the effects of the dead volume geometry (length and diameter) and axial dispersion inside dead volume on SMB modeling and simulation. Since the axial dispersion inside dead volume considerably affects the SMB performance, there remains the need to consider the actual dead volume geometry in industrial scale SMB.

The purpose of this study is to examine how the geometry of dead volume influences concentration dynamics and flushing performance in a 7-zone PX SMB unit in the presence of axial dispersion inside dead volume. This paper is organized as follows: the 7-zone PX SMB unit of an industrial scale is presented in Sect. 2. The one-dimensional unsteady-state SMB model is summarized for the adsorption column and the dead volume in Sect. 3. Here, the geometric factor of dead volume is derived from the Peclet number appearing in the dimensionless differential equation for dead volume. In Sect. 4, optimal flushing flow rates of the 7-zone PX SMB are obtained from the parametric study, considering the geometric factor of dead volume. This study demonstrated that a complex geometry of dead volume can be modeled into a simple geometry by using the geometric factor to ensure the same flow patterns inside dead volume, providing a reliable result from the unsteady-state one-dimensional (1D) SMB model.

2 Seven-zone PX SMB and dead volumes

The PX SMB separates PX from its C_8 aromatic isomers using p-diethylbenzene (PDEB) as a desorbent (D) (Minceva and Rodrigues 2002). The process is designed to recover more than 97 wt% of PX from the feed with a minimum extract purity of 99.7 wt% (UOP 2010). The 7-zone PX SMB is designed to prevent the accumulation of impurities in the bed-lines, especially to wash out extract bed-line contamination by xylene isomer residue from the previous feed stream. The 7-zone SMB has two flushing sequences i.e., line flush flows (LF) and a secondary flush inlet-flow (SF_i) which uses a medium that does not affect extract purity. The detail about the 7-zone PX SMB is found elsewhere (Lim et al. 2010; Minceva and Rodrigues 2003).

Figure 1 shows a schematic diagram of the 7-zone PX SMB unit with 24 adsorption beds and 24 bed-lines. The rotary valve shifts the injection and withdrawal ports by one-bed ahead. The pump provides liquid circulation from the

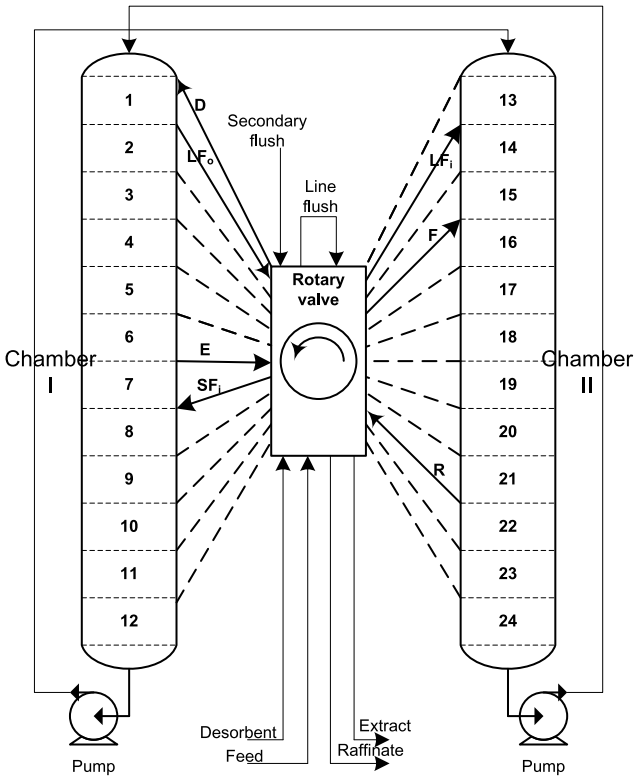

Fig. 1 Schematic diagram of 7-zone PX SMB process (LF_o: line flush outlet, E: extract, SF_i: secondary flush inlet, LF_i: line flush inlet, F: feed, R:raffinate)

bottom of a chamber to the top of another one. The location of the LF and SF_i ports is designed in such a way to give the best performance. In this study, both of the extra-column dead volumes (bed-head and bed-tail) (Katsuo et al. 2009; Migliorini et al. 1999) and bed-line dead volumes (Lim et al. 2010; Minceva and Rodrigues 2003) were taken into account. The simplified geometries of the dead volumes are illustrated in Fig. 2 for the 12th and 13th beds of the 7-zone SMB. A wide and short bed-head (BH) is located at the top of the bed, while a very long bed-tail (BT) is equipped to connect the two chambers only at the bottom of 12th and 24th beds. Only the 7 bed-lines (BL) are active in transporting the liquid from/to the beds and to/from the rotary valve at each shifting.

Table 1 reports the column configuration, geometries (diameter and length) of beds, bed-heads, bed-tails, and bed-lines, operating conditions, SMB model parameters, and the computational parameters used in this study. The bed-head has the same diameter (d_{BH}) as the column diameter (d_c) with 0.02 m in length (L_{BH}) for all the beds. The bed-tail diameter (d_{BT}) is 0.3048 m with the length (L_{BT}) of 21.71 m. The bed-line volume (V_{BL}) is set to be 0.145 m^3 (1 % of the bed volume) for all beds, and its diameter (d_{BL}) is 0.2028 m. The flow rates of desorbent (Q_D), extract (Q_E), feed (Q_F), and recycle ($Q_{recycle}$) were taken

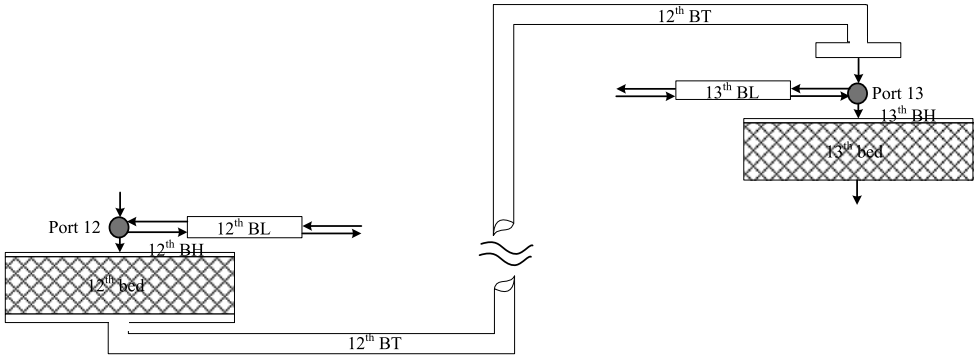

Fig. 2 Schematic diagram for 12th and 13th beds of PX SMB with simplified geometries for BH (bed-head), BT (bed-tail), and BL (bed-line)

Table 1 Simulation parameters for 7-zone p-xylene SMB process

Design parameters			
bed configuration	1-5-1-6-2-6-3	L_{BH} (m)	0.02 for each bed-head
L_c (m)	1.1	d_{BH} (m)	4.1 for each bed-head
d_c (m)	4.1	L_{BT} (m)	21.71 only for 12th and 24th bed
ρ_p (kg/m^3)[a]	2279	d_{BT} (m)	0.3048 only for 12th and 24th bed
ε_b	0.39	V_{BL} (m^3)	0.145 for each bed-line
		d_{BL} (m)	0.2028 for each bed-line
Operating parameters			
Q_D (m^3/min)	2.89	Components (5)	PX (product), MX, OX, EB, PDEB (desorbent)
$Q_{LFo} = Q_{LFi}$ (m^3/min)	0.15	C_F (kg/m^3)	171, 360, 92, 101, 0
Q_E (m^3/min)	1.8	C_D (kg/m^3)	0, 0, 0, 0, 724
Q_{SFi} (m^3/min)	0.15	C_{SFi} (kg/m^3)	0, 0, 0, 0, 724
Q_F (m^3/min)	1.45	τ (min)	1.15
Q_R (m^3/min)	2.69	N_{shift}	480 (20 cycles)
$Q_{recycle}$ (m^3/min)	5.39		
Model parameters			
D_{ax} (m^2/min)	$0.58 \times 10^{-3} v_L$	Pe	2,000
$D_{ax,BH}$ (m^2/min)	$340 \times 10^{-3} v_{L,BH}$	Pe_{BH}	0.095
$D_{ax,BT}$ (m^2/min)	$20 \times 10^{-3} v_{L,BT}$	Pe_{BT}	1,500
$D_{ax,BL}$ (m^2/min)	$15 \times 10^{-3} v_{L,BL}$	Pe_{BL}	375
k_i (min^{-1})	2.0 for each component	Re_{BH}	9000
a_i (–)[b]	0.139 0.03 0.025 0.04 0.139	Re_{BT}	1,945,000
b_i (m^3/kg)	1.07 0.23 0.19 0.31 1.29	Re_{BL}	1,000,000
ρ (kg/m^3)	724.7	μ (kg/m/s)	2.08×10^{-4}
Computational parameters			
N_{mesh}	24	N_{time}	80
Δz (m)	0.046	Δt (min)	0.014
$N_{CFL,max}$	0.465		

[a] Apparent particle density: $\rho_p = \rho_{bulk}/(1 - \varepsilon_b)$

[b] $a_i = q_{max,i} \cdot b_i$ where q_{max} [kg/m^3] is the maximum adsorbed concentration

from Minceva and Rodrigues (2003). The flow rates of line flush (Q_{LF}) and secondary flush-inlet (Q_{SFi}) are set for being able to flush 120 % (0.15 m^3/min) of V_{BL} during the shifting time ($\tau = 1.15$ min). The Q_{LFi} should be the same as the Q_{LFo}, forming an internal recycle loop. The raffinate flow rate (Q_R) is calculated on the basis of the total mass balance.

$$Q_F + Q_D + Q_{SFi} = Q_E + Q_R \tag{1}$$

The inlet concentrations of feed (C_F), desorbent (C_D) and secondary flush (C_{SFi}) are given for the five components of which PX is the product, PDEB is the desorbent, and meta-

xylene (MX), ortho-xylene (OX), and ethylbenzene (EB) are impurities. The density of PX (= 712 kg/m^3) is a little lower than that of PDEB (= 724 kg/m^3) at an operating temperature of 177 °C. The Langmuir adsorption isotherm parameters (a_i and b_i) were adopted from Minceva and Rodrigues (2003). The simulation results were analyzed after 480 shiftings (or 20 cycles).

3 Unsteady-state SMB model

The SMB process is modeled by connecting an adsorptive bed model and a non-adsorptive dead volume model, while considering the periodic port shifting in SMB operation through the extended node model (Lim et al. 2010). The extended node model is applied to port shifting involving the streams of BH, BT and BL (Lim et al. 2010).

3.1 Adsorptive SMB model

The adsorption bed is represented by a convection-diffusion-reaction partial differential equation (PDE) with linear driving force (LDF) mass transfer and competitive Langmuir adsorption isotherms (Beste et al. 2000; Dünnebier and Klatt 2000; Kurup et al. 2005; Lim and Bhatia 2011; Lim and Jorgensen 2004; Lim et al. 2010; Minceva and Rodrigues 2003). This one-dimensional (1D) SMB model assumes that the bed void fraction, particle radius and porosity are constant along the columns, the mass transfer coefficients are independent of the mixture composition, the thermal effect and pressure drop of beds are negligible, as well as the hydrodynamics are ignored in the radial direction

$$\frac{\partial C_i}{\partial t} + v_L \frac{\partial C_i}{\partial z} = \frac{\partial}{\partial z}\left(D_{ax}\frac{\partial C_i}{\partial z}\right) - \frac{1-\varepsilon_b}{\varepsilon_b} k_i \rho_p \left(n_i^* - n_i\right) \tag{2}$$

$$\frac{dn_i}{dt} = k_i\left(n_i^* - n_i\right) \tag{3}$$

$$n_i^* = \frac{a_i \cdot C_i}{1 + \sum_j b_j C_j} \tag{4}$$

where v_L (m/min) is the interstitial velocity assumed to be constant within the bed, D_{ax} (m^2/min) is the axial dispersion coefficient, ε_b is the bed voidage, k_i (min^{-1}) is the mass transfer coefficient for each component (i), ρ_p (kg-adsorbent/m^3-adsorbent) is the apparent solid density, C_i (kg/m^3-fluid) is the liquid concentration, n_i (kg/kg-adsorbent) is the solid concentration, and n_i^* (kg/kg-adsorbent) is the equilibrium concentration defined by Langmuir adsorption isotherms which have two parameters (a_i and b_i) for each component. In this study, the axial dispersion coefficient (D_{ax}) is assumed to be proportional to the interstitial fluid velocity (v_L)

$$D_{ax} = L_{diff} \cdot v_L \tag{5}$$

where L_{diff} (m) is the axial dispersion intensity factor.

Two initial conditions (IC, $t = 0$) for the two time derivatives and two boundary conditions (BC, $z = 0$ and L_c) for the convection and diffusion terms are required to solve Eqs. (2)–(3)

$$IC = \begin{cases} C(z,0) = C_{initial}(t=0,\forall z) \\ n(z,0) = n_{initial}(t=0,\forall z) \end{cases} \tag{6}$$

$$BC = \begin{cases} v_L(C_{z=0} - C_{in}) = L_{diff} \times v_L \frac{dC}{dz}\big|_{z=0}, & \forall t \\ \frac{dC}{dz}\big|_{z=L_c} = 0, & \forall t \end{cases} \tag{7}$$

where C_{in} is the inlet concentration entering the column which is determined by operating conditions (or calculated by the extended node model)

3.2 Dead volume model

The non-adsorptive (or dead volume) region is conceptualized by the bed-head (BH), the bed-tail (BT), and the bed-line (BL). This study assumes that the thermal effect, pressure drop, and radial mixing inside dead volume are negligible. The dead volume is modeled by the 1D convection-diffusion model (Jin and Wankat 2007; Katsuo et al. 2009; Lim and Bhatia 2011; Lim et al. 2010; Minceva and Rodrigues 2003; Zabka et al. 2008):

$$\frac{\partial C_i}{\partial t} + v_{dead}\frac{\partial C_i}{\partial z} = D_{ax,dead}\frac{\partial^2 C_i}{\partial z^2} \tag{8}$$

where v_{dead} is the superficial velocity of the fluid and $D_{ax,dead}$ is the axial dispersion coefficient in BH, BT and BL. The axial dispersion coefficient of dead volume ($D_{ax,dead}$) is also assumed to be:

$$D_{ax,dead} = L_{diff,dead} \cdot v_{dead} \tag{9}$$

where $L_{diff,dead}$ is the axial dispersion intensity factor of dead volume. The convection-diffusion model inside dead volume is completed with the commonly used initial and boundary conditions

$$IC = C(z,0) = C_{initial}(t=0,\forall z) \tag{10}$$

$$BC = \begin{cases} v_{dead}(C_{z=0} - C_{in}) \\ \quad = L_{diff,dead} \times v_{dead}\frac{dC}{dz}\big|_{z=0}, & \forall t \\ \frac{dC}{dz}\big|_{z=L_{dead}} = 0, & \forall t \end{cases} \tag{11}$$

where C_{in} is the inlet concentration entering the dead volume and L_{dead} is the length of dead volume.

3.3 Geometric factor in dead volume model

The transfer line geometry, the physical property of fluid, and the flow rate determine the flow pattern inside dead volume (Levenspiel 1999; Nauman 2001; Fogler 2005). In the dimensionless form with $x = z/L_{dead}$ and $\theta = \frac{t \cdot v_{dead}}{L_{dead}}$, Eq. (8) becomes:

$$\frac{dC_i}{d\theta} = \left(\frac{D_{ax,dead}}{v_{dead} \cdot L_{dead}}\right)\frac{d^2C_i}{dx^2} - \frac{dC_i}{dx} \tag{12}$$

where the dimensionless group $(\frac{D_{ax,dead}}{v_{dead} \cdot L_{dead}})$ is the inverse of the dead volume Peclet number (Pe_{dead}) which may be determined by Levenspiel's method through the graphical correlation to the Reynolds number (Re) (Fogler 2005; Levenspiel 1999).

$$\left(\frac{D_{ax,dead}}{v_{dead} \cdot L_{dead}}\right) = \frac{1}{Pe_{dead}} \tag{13}$$

Equation (12) signifies that the concentration dynamics inside dead volume are identical for the same Peclet number.

Actual dead volume geometry can be complex with different diameters for bending, enlargement, reduction, or connection parts. When the actual dead volume is modeled in 1D SMB simulation, the complex geometry is often simplified to have a representative diameter with the same volume (V_{dead}) and flow rate (Q) as the original ones, as illustrated in Fig. 3. The actual dead volume with three different diameters (d_{1a}, d_{1b}, and d_{1c}) and lengths (L_{1a}, L_{1b}, and L_{1c}) is simplified into a single tube with a diameter (d_2) and a length (L_2). Even though the two geometries are completely different, their concentration profiles at the end of the tube should be identical, which is achieved by setting the same Pe_{dead} number according to Eq. (12).

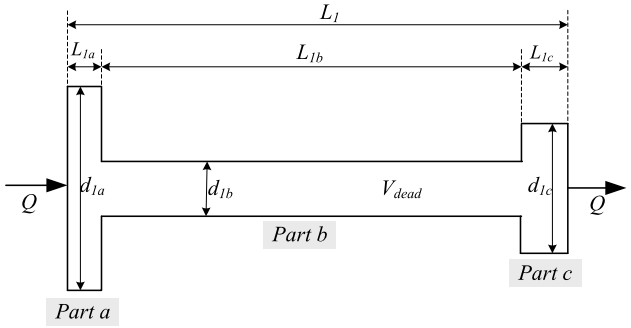

a) Dead volume with a given geometry

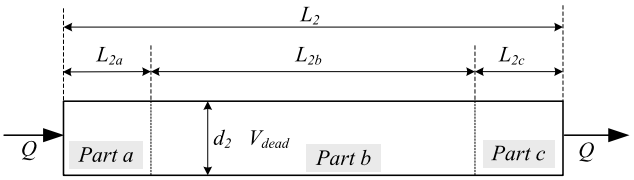

b) Dead volume with a simplified geometry

Fig. 3 Simplification of dead volume geometry keeping the same flow rate (Q) and volume (V_{dead})

For the same flow rate (Q), the Pe number for dead volume is defined as:

$$Pe_{dead} = \frac{v_{dead} \cdot L_{dead}}{D_{ax,dead}} = \frac{4L_{dead}Q}{\pi d_{dead}^2 \cdot D_{ax,dead}} \tag{14}$$

Changing the diameter (d_1 into d_2) and length (L_1 into L_2) but keeping the same volume (V_{dead}) and Pe_{dead}, the axial diffusion ratio between the two different geometries is:

$$\frac{D_{ax,dead,2}}{D_{ax,dead,1}} = \frac{L_2}{L_1}\left(\frac{d_1}{d_2}\right)^2 = \left(\frac{d_1}{d_2}\right)^4 = \left(\frac{L_2}{L_1}\right)^2 \tag{15}$$

Equation (15) indicates the shape factor of axial dispersion to obtain the same concentration profiles, when the geometry of dead volume changes. Combining Eqs. (9) and (15), the following shape factor of dead volume axial dispersion intensity ($L_{diff,dead}$) is derived by keeping the same Pe_{dead} number:

$$\frac{L_{diff,dead,2}}{L_{diff,dead,1}} = \frac{L_2}{L_1} = \left(\frac{d_1}{d_2}\right)^2 \tag{16}$$

It is noted that Eqs. (15) and (16) are valid only when the radial hydrodynamics are ignored. However, once a lumped dispersion coefficient considering both axial and radial mixing effects is determined, the geometric factor is applicable to practical systems.

Figure 3 illustrates a given geometry divided into three parts and a simplified geometry having the same diameter for the three parts. Figure 3(a) represents the shape of bed-tail in Fig. 2, where Part a corresponds to the bottom of the bed, Part b is the long tube connecting the two chambers, and the part of flow distribution is simplified into Part c. The total lengths of the given and simplified geometries are L_1 and L_2. Since the two geometries have the same volume (V_{dead}) and flow rate (Q), the times required for fluid to pass through the two tubes are the same.

For the given geometry of Fig. 3(a), the convection-diffusion model is described as follows:

$$\begin{aligned}
&\frac{\partial C_i}{\partial t} + v_{1a}\frac{\partial C_i}{\partial z} = L_{diff,1a}v_{1a}\frac{\partial^2 C_i}{\partial z^2}, \quad 0 \le z < L_{1a} \\
&\frac{\partial C_i}{\partial t} + v_{1b}\frac{\partial C_i}{\partial z} = L_{diff,1b}v_{1b}\frac{\partial^2 C_i}{\partial z^2}, \\
&\quad L_{1a} \le z < L_{1a} + L_{1b} \\
&\frac{\partial C_i}{\partial t} + v_{1c}\frac{\partial C_i}{\partial z} = L_{diff,1c}v_{1c}\frac{\partial^2 C_i}{\partial z^2}, \quad L_{1a} + L_{1b} \le z \le L_1
\end{aligned} \tag{17}$$

where v_{1a}, v_{1b}, and v_{1c} are the fluid velocities of the first, second and third parts, respectively. $L_{diff,1a}$, $L_{diff,1b}$, and $L_{diff,1c}$ are the dispersion intensities of these three parts, respectively. The dead volume model of Fig. 3(b) is formulated with the help of Eq. (16):

$$\frac{\partial C_i}{\partial t} + v_2 \frac{\partial C_i}{\partial z} = L_{diff,1a}\left(\frac{L_{2a}}{L_{1a}}\right) v_2 \frac{\partial^2 C_i}{\partial z^2}, \quad 0 \le z < L_{2a}$$

$$\frac{\partial C_i}{\partial t} + v_2 \frac{\partial C_i}{\partial z} = L_{diff,1b}\left(\frac{L_{2b}}{L_{1b}}\right) v_2 \frac{\partial^2 C_i}{\partial z^2}, \quad L_{2a} \le z < L_{2a} + L_{2b} \tag{18}$$

$$\frac{\partial C_i}{\partial t} + v_2 \frac{\partial C_i}{\partial z} = L_{diff,1c}\left(\frac{L_{2c}}{L_{1c}}\right) v_2 \frac{\partial^2 C_i}{\partial z^2}, \quad L_{2a} + L_{2b} \le z \le L_2$$

where v_2 is the fluid velocity in the tube for the simplified geometry. Equations (17) and (18) are identical, as the shape factor is employed to the dispersion intensity of the simplified geometry so that the Peclet numbers of the two different geometries are the same. Equation (18) expressed for the same diameter (d_2) and velocity (v_2) may be reduced again into one equation with the dispersion intensity averaged over the whole length (L_2):

$$\frac{\partial C_i}{\partial t} + v_2 \frac{\partial C_i}{\partial z} = L_{diff,mean} v_2 \frac{\partial^2 C_i}{\partial z^2}, \quad 0 \le z < L_2 \tag{19}$$

where the arithmetic mean dispersion intensity ($L_{diff,mean}$) is defined as:

$$L_{diff,mean} = \frac{1}{L_2}\left[L_{diff,1a}\left(\frac{L_{2a}}{L_{1a}}\right)L_{2a} + L_{diff,1b}\left(\frac{L_{2b}}{L_{1b}}\right)L_{2b} + L_{diff,1c}\left(\frac{L_{2c}}{L_{1c}}\right)L_{2c}\right] \tag{20}$$

The geometric mean dispersion intensity can be also used:

$$L_{diff,mean} = \frac{1}{L_2}\left[L_{diff,1a}\left(\frac{L_{2a}}{L_{1a}}\right)L_{2a} \times L_{diff,1b}\left(\frac{L_{2b}}{L_{1b}}\right)L_{2b} \times L_{diff,1c}\left(\frac{L_{2c}}{L_{1c}}\right)L_{2c}\right]^{\frac{1}{3}} \tag{21}$$

It is noted that Eq. (19) can be used with a limited accuracy, because Eq. (18) and Eq. (19) are not identical but Eq. (19) mimics Eq. (18). When the tube length (L) or the dispersion intensity (L_{diff}) of one part is much greater than that of the other parts, there would be little difference between Eqs. (18) and (19).

Even though the actual complex geometry of dead volume can be simplified into a representative geometry, it is still required to determine the dispersion intensity (L_{diff}) for the original geometry in solving the dead volume model. As mentioned earlier, *Pe* may be a function of *Re* (Fogler 2005; Levenspiel 1999). For a given Q and V_{dead}, the *Re* number is defined as:

$$Re = \frac{\rho v_{dead} d_{dead}}{\mu} = \frac{4\rho Q}{\pi \mu d_{dead}} \tag{22}$$

where the density (ρ) and the viscosity (μ) are assumed to be constant. Because the flow rates (Q) and the diameters (d_{dead}) of BH, BT, and BL are different, they have different Reynolds numbers (see Table 1). Employing the Levenspiel method (Fogler 2005; Levenspiel 1999) to obtain *Pe* as a function of *Re*, the axial dispersion coefficients ($D_{ax,dead}$), *Pe* and *Re* for BH, BT, and BL are given in Table 1, where $D_{ax,dead}$ was calculated as:

$$D_{ax,dead} = \frac{L_{dead}}{Pe_{dead}} \cdot v_{dead} \tag{23}$$

Table 2 reports the simulation parameters to numerically confirm whether Eqs. (17), (18), and (19) are identical. The flowrate (Q) is set to 3.0 m^3/min. The given shape corresponding to the bed-tail in Fig. 2 has three diameters (4.0, 0.3, and 1.0 m) and lengths (0.01, 15, and 0.5 m) in series. The diameter of the simplified geometry is set to 0.3 m. The length of the simplified geometry is calculated so that the volume of the simplified geometry is the same as that of the given geometry. The Reynolds numbers (*Re*) are obtained by using density (ρ) and viscosity (μ) reported in Table 1 for xylene isomers. The inlet feed concentration (C_{in}) was given to 160 kg/m^3 only for the first 30 seconds and the initial concentration ($C_{initial}$) was zero for the whole range. The

Table 2 Simulation parameters to solve convection-diffusion model of a tube

Parameters	Eq. (17)			Eq. (18)			Eq. (19)
	Part a	Part b	Part c	Part a	Part b	Part c	
Q (m^3/min)	3.0			3.0			3.0
ΔL (m)	0.0310			0.0447			0.0447
d (m)	4.0	0.3	1.0	0.3			0.3
L (m)	0.01	15	0.5	1.78	15	5.56	22.33
v (m/s)	0.0040	0.7074	0.0637	0.7074			0.7074
t (s)	2.51	21.21	7.85	2.51	21.21	7.85	31.57
Re (–)	5.55×10^4	7.39×10^5	2.22×10^5	7.39×10^5			7.39×10^5
L_{diff} (m)	0.092	0.004	0.015	16.36	0.004	0.1667	0.0525
D_{ax} (m^2/s)	0.0004	0.0028	0.0010	11.57	0.0028	0.1179	0.0372

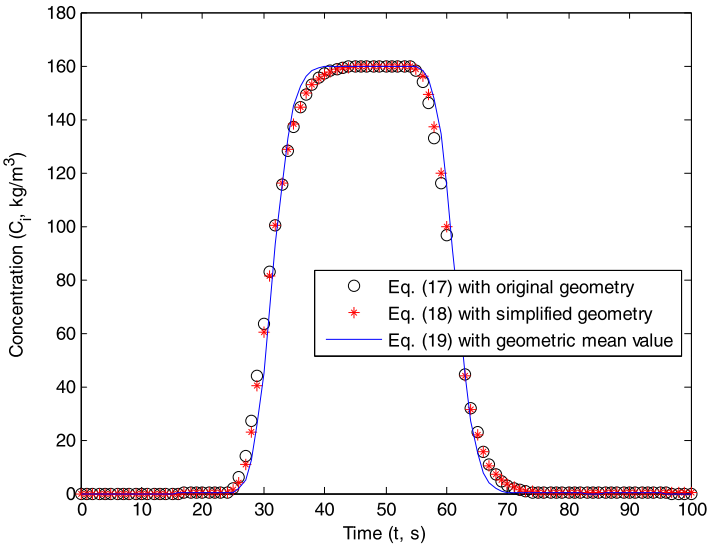

Fig. 4 Concentration profiles (C_i) at the end of tube with respect to time (t)

dispersion intensities (L_{diff}) for the given geometry were estimated from the Levenspiel method. Those of the simplified geometry were calculated from Eq. (16). The dispersion intensity used in Eq. (19) was computed from Eq. (21). The total length (L) for the two geometries was divided into 501 points in order to convert the partial differential equation to a set of ordinary differential equations with time. The second-order and first-order spatial derivatives were discretized by the central and upwind schemes, respectively. The spatial step size (ΔL) is indicated in Table 2.

Figure 4 demonstrates that Eqs. (17) and (18) are equivalent mathematically. However, the concentration profile of Eq. (19) with the geometric mean intensity factor shows a little difference from those of Eqs. (17) and (18). As mentioned earlier, Eq. (19) can be used within a certain range of accuracy. It is evident that the same concentration profiles with respect to time are obtained for any different tube geometry, as long as the shape factor is applied to convert the axial dispersion coefficient.

3.4 Comparison of this study with other approaches

Table 3 compares our approach with previous studies in terms of the type, the geometry, and the model of dead volume. Both the extra-column and bed-line dead volumes are considered in Lim et al. (2010) and the present work. Over-simplified dead volume geometries were used in Lim et al. (2010), while the present study applies realistic geometries of dead volume and the shape factor for axial dispersion.

The node mass balances without axial dispersion were used to describe concentration dynamics of fluid passing through an empty tube of dead volume (Minceva and Rodrigues 2003). The convection-diffusion model has been widely adopted for the dead volume model (Katsuo et al. 2009; Lim et al. 2010; Zabka et al. 2008; Jin and Wankat 2007). The axial dispersion coefficient was determined by the graphical Levenspiel's correlation (Levenspiel 1999) for a laminar flow (Zabka et al. 2008) and for a turbulent flow (Jin and Wankat 2007). In this study, the axial dispersion coefficient for each dead volume is obtained from the Levenspiel correlation for turbulent flow.

4 Simulation results for 7-zone PX SMB

A 7-zone PX SMB with the parameters listed in Table 1 is taken for the case study. The calculation was performed on a personal computer (two cores of Duo CPU of 2.2 GHz with 3 GB RAM) using a fast and accurate solution tool for chromatography and SMB (FAST-Chrom/SMB) (Lim and Bhatia 2011; Lim et al. 2010; Lim and Jorgensen 2004).

4.1 Three case studies

The geometries (d_{dead}) and axial dispersion intensities ($L_{diff,dead}$) of bed-line and bed-tail are given for three case studies in Table 4. Case I represents an SMB simulation with the nominal parameters in Table 1. The $L_{diff,dead}$ of Case I was obtained from the Levenspiel correlation (Levenspiel 1999) for the BH, BT, and BL with the nominal geometries and the average flow rates. In Cases II and III, the diameters of BT (d_{BT}) and BL (d_{BL}) are enlarged to 4.1 m and the lengths are shortened to keep the same BT and BL volumes as those of Case I. The BH geometries of Cases II and III are set to be the same as those of Case I. Case II has the same dead volume axial dispersion intensity ($L_{diff,dead}$) as Case I, ignoring the geometric factor even though the diameters of BL and BT are different. The geometric factor in Eq. (16) is applied for Case III to convert the dead volume axial dispersion intensities ($L_{diff,dead}$) of BT and BL.

Table 3 Literature survey on dead volume treatment in SMB modeling

Articles	Dead volume type		Dead volume geometry	Dead volume model
	Extra-column	Bed-line		
Minceva and Rodrigues (2003)	no	yes	–[a]	Node mass balance without axial dispersion.
Jin and Wankat (2007)	yes	No	Tube of heat exchanger.	Convection-diffusion model where the $D_{ax,dead}$ was determined by Levenspiel's graphical correlation for turbulent region.
Zabka et al. (2008)	yes	No	Tube before column which increases the residence time (Licosep model).	Convection-diffusion model where the $D_{ax,dead}$ was determined by Levenspiel's correlation for laminar flow.
Katsuo et al. (2009)	yes	No	Tube before column which increases the residence time.	Convection-diffusion model where the $D_{ax,dead}$ was determined in terms of numerical dispersion.
Lim et al. (2010)	yes	yes	Tube before adsorptive bed (BH), tube after adsorptive bed (BT), and tube of bed-line (BL). All of the tubes have the same diameter as that of adsorptive bed.	Convection-diffusion model where the same axial dispersion of dead volumes ($= 5 \times 10^{-3} \times v_L$ m^2/min) was used.
Present work	yes	yes	Tube before adsorptive bed (BH), tube after adsorptive bed (BT), and tube of bed-line (BL). Dead volume geometric factor is considered.	Convection-diffusion model where the $D_{ax,dead}$ for BH, BT, and BL are determined by Levenspiel's graphical correlation (turbulent region).

[a]The transfer line without specific dead volume geometry is modeled as a node having concentration values in three different time stages during one switching period

Table 4 Effects of dead volumes geometry on SMB performance

Case studies	Mass balance deviation (%)	Purity (%)	Recovery (%)
Case I			
$d_{BL} = 0.2028$ m and $d_{BT} = 0.3048$ m $L_{diff,BH}, L_{diff,BT}, L_{diff,BL} = (340, 20, 15) \times 10^{-3}$ m	1.43	99.27	97.57
Case II			
$d_{BL} = 4.1$ m and $d_{BT} = 4.1$ m $L_{diff,BH}, L_{diff,BT}, L_{diff,BL} = (340, 20, 15) \times 10^{-3}$ m	1.28	99.96	95.33
Case III			
$d_{BL} = 4.1$ m and $d_{BT} = 4.1$ m $L_{diff,BH}, L_{diff,BT}, L_{diff,BL} = (340, 0.11, 0.036) \times 10^{-3}$ m	1.45	99.25	97.59

Two process performances, namely purity and recovery, were evaluated for each case. The extract purity was calculated without considering the desorbent concentration ($C_{E,PDEB}$).

$$\text{Purity } (\%) = 100 \times \frac{\bar{C}_{E,PX}}{\bar{C}_{E,PX} + \bar{C}_{E,MX} + \bar{C}_{E,OX} + \bar{C}_{E,EB}} \tag{24}$$

where $\bar{C}_{E,i}$ is the time-averaged concentration of fluid component i in the extract. The recovery of PX was determined by the ratio of the PX amount in the extract to that of the inlet feeding.

$$\text{Recovery } (\%) = 100 \times \frac{\bar{C}_{E,PX} \cdot Q_E}{Q_F \cdot C_{F,PX}} \tag{25}$$

It is worth noting that the mean concentrations (e.g., $\bar{C}_E$) no longer reach a steady-state but a cyclic steady-state (see Fig. 5) because of the non-homogeneous length of the bed-tails. The one-shifting averaged PX concentration in extract reaches a cyclic steady-state after about 10 cycles (240 shift-

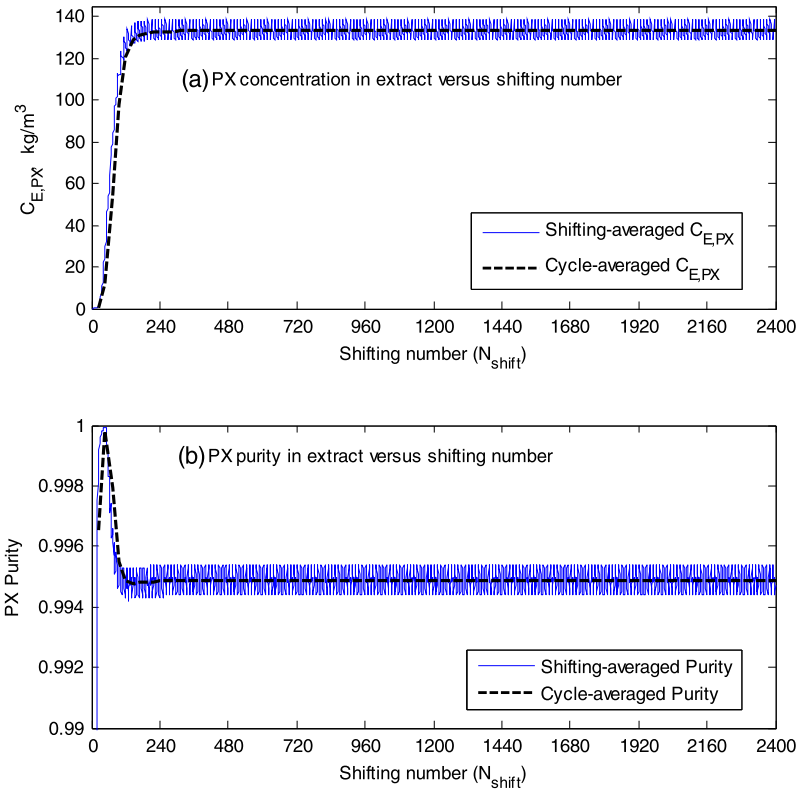

Fig. 5 Mean concentration ($C_{E,PX}$) and purity in extract with respect to the number of shifting (N_{shift})

ings) and little change is observed after 360 shiftings, as shown in Fig. 5(a). The one-cycle averaged concentration shows a steady-state after 360 shiftings. The extract purity has the same behavior as the PX concentration. After overshooting at the beginning moment, the one-cycle averaged purity keeps constant and stable, as illustrated in Fig. 5(b).

Therefore, the 480 shiftings were good enough to reach a stable cyclic steady state at the operating conditions. The mean concentrations time-averaged over the last cycle (from 457 to 480 shiftings) were taken for the SMB performance evaluation.

The mass balance deviation of PX for each case is calculated as follows:

$$\text{Error } (\%) = 100\frac{C_{F,PX}\cdot Q_F - (\bar{C}_{E,PX}\cdot Q_E + \bar{C}_{R,PX}\cdot Q_R)}{C_{F,PX}\cdot Q_F} \tag{26}$$

where $\bar{C}_{PX}$ is the time-averaged PX concentration over the last cycle (from 457 to 480 shiftings). The mass balance deviations of the three cases are below 1.5 % (see Table 4), which may be highly accurate solutions to our knowledge.

Table 4 indicates that the purity and recovery of Case I are quasi identical to those of Case III, as the shape factor of Eq. (16) was applied to Case III. A slight discrepancy of purity and recovery between the two cases is found because of the numerical instability caused by the huge amount of iterative calculations to solve the PDE system. It is evident in Table 4 that the simulation results of Case I are significantly different from those of Case II, showing higher purity and lower recovery.

Figure 6 verifies that Cases I and III have the almost same concentration profiles of PX at the end of the extract bed-line. As expected, the concentration profile during the last shifting time of Case II is different from that of Case I/III. Since the collaboration of LF and SF_i cleaned up the extract bed-line in the previous shifting, no PX comes out during the initial moment (about 0.08 min) taken for passing through the bed-line (see Case I/III in Fig. 6). The concentration profile of Case II is more dispersed than those of Case I/III, because the diffusivity of Case II is not corrected properly even though the velocities inside bed-line and bed-tail were converted correctly in Case II (see also Table 4).

4.2 Optimal flushing flow rates in 7-zone PX SMB

Figure 7a depicts the parametric study of Q_{LF} and Q_{SFi} on purity and recovery for Case I/III, while the parametric study for Case II is displayed in Fig. 7b. The feasible areas where purity is over 99.7 % are indicated in Fig. 7. Optimal flushing flow rates are obtained for Case I/III and Case II, maximizing recovery within the feasible area. The surfaces of purity and recovery much depend on the dead volume geometry, as shown in Fig. 7. Thus, the geometric factor has to be applied correctly when the geometry of dead volume is simplified.

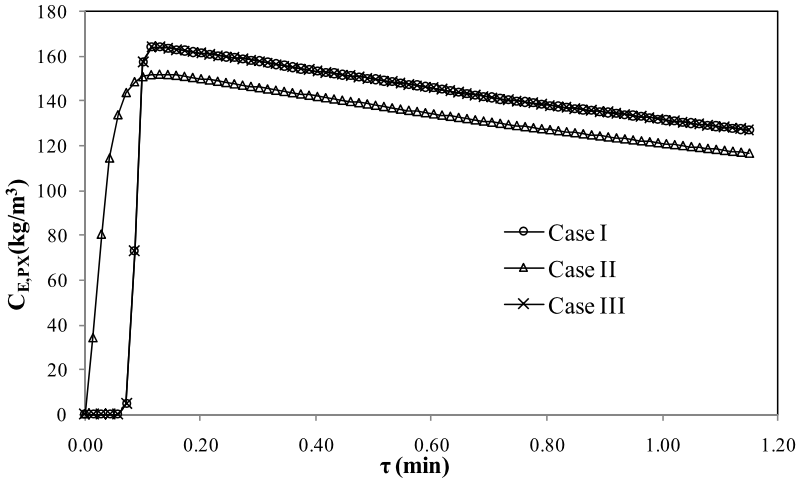

Fig. 6 Comparison of PX concentration profiles at the end of extract bed-line during the last shifting for Cases I, II and III

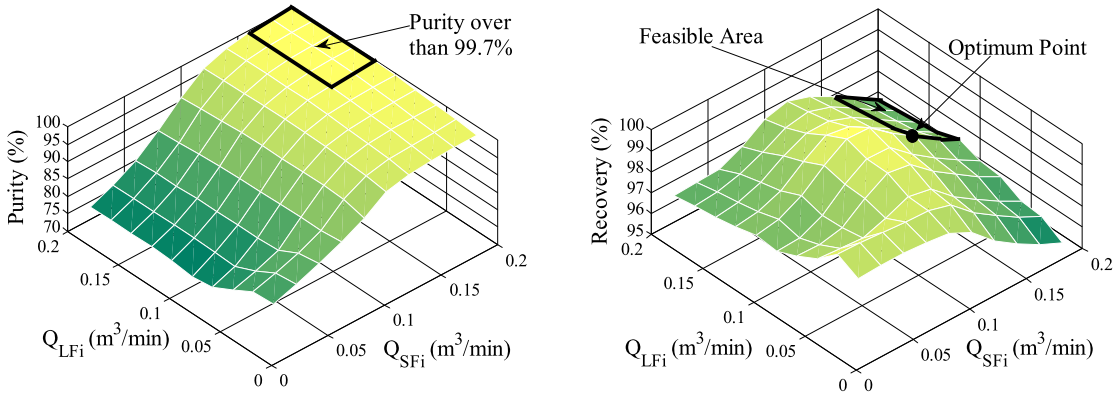

a) Q_{LF} and Q_{SFi} effect on purity and recovery at Case I and III

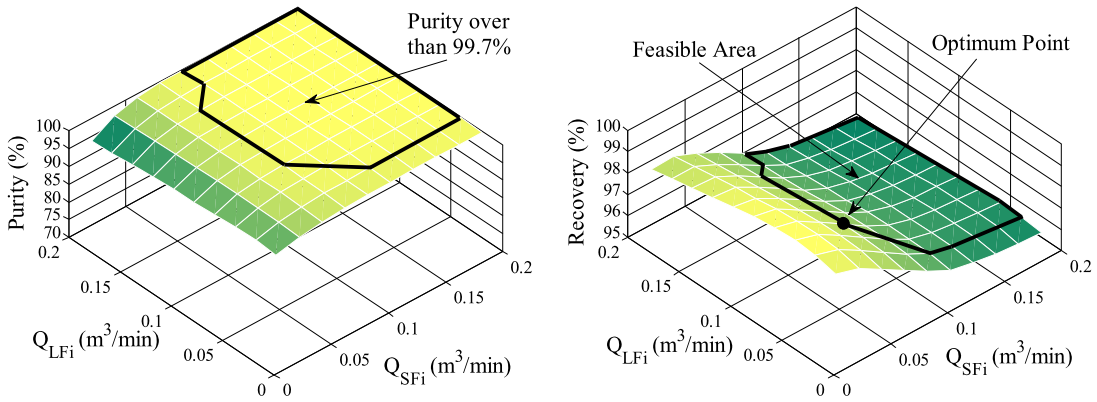

b) Q_{LF} and Q_{SFi} effect on purity and recovery at Case II

Fig. 7 Parametric study of two variables (Q_{LF} and Q_{SFi}) on purity and recovery

Table 5 compares flushing flow rates, purity, and recovery of Case I/III with those of the two optimized cases. The optimized cases satisfy the purity constraint at the cost of recovery. Because the axial dispersion intensities of the optimized Case II were not correctly converted (see Table 4), the optimal flushing flow rates are out of practical application. The

Table 5 Comparison of flushing flow rates, purity, and recovery among Case I/III and two optimized cases

Simulation	Line flushing		Secondary flushing		Purity (%)	Recovery (%)
	Q_{LF} (m^3/min)	V_{BL} Ratio (%)	Q_{SFi} (m^3/min)	V_{BL} Ratio (%)		
Case I/III	0.15	120	0.15	120	99.27	97.57
Optimized Case I/III	0.12	95	0.175	139	99.70	97.13
Optimized Case II	0.08	63	0.08	63	99.72	97.14

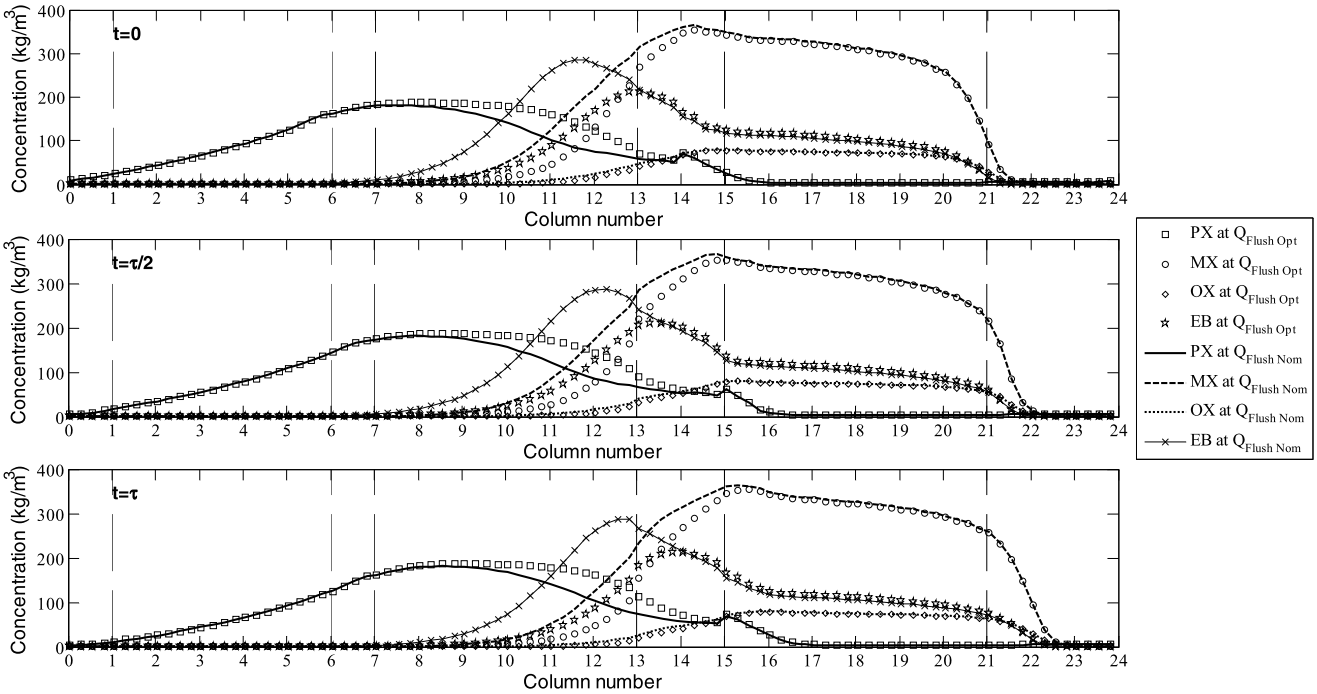

Fig. 8 Comparison of liquid concentration distributions between optimized case (*points*) and Case I/III (*lines*) at three different times during the last shifting period

flushing flow rates of the optimized case I/III are regarded as a valid operating condition. The ratio of the flushing flow rate to the bed-line dead volume (V_{BL} ratio, %) is calculated as:

$$V_{BL}\ \text{Ratio} = 100 \times \frac{\tau \cdot Q_{LF\ or\ SF_i}}{V_{BL}} \tag{27}$$

In the optimized case I/III, a relatively low Q_{LF} (0.12 m^3/min or 95 %) and a high Q_{SFi} (0.175 m^3/min or 139 %) are obtained.

Figure 8 displays concentration profiles along the bed number for the optimized and the nominal flushing flow rates of Case I/III at three different times (i.e., beginning, middle and last moments) during the last shifting period. The optimized profiles (points in Fig. 8) are moved a little to the right in zones 4 and 5, compared to the nominal ones (lines in Fig. 8), because the optimized Q_{SFi} is higher than the nominal one to meet 99.7 % of purity. However, that results in a lower recovery than the nominal one.

LF and SF_i correlate with each other and work as a sequence to prevent extract contamination by flushing the bed-line which was previously used as the feed bed-line. Hence, an appropriate amount of Q_{LF} and Q_{SFi} increases extract purity and recovery. Since excessive Q_{LF} reduces the flow rates of zones 2, 3, and 4, recovery deteriorate within the feasible region, as observed in Fig. 7. Excessive Q_{SFi} causes PX loss through the raffinate port, which reduces recovery. The sensitivity of recovery on Q_{SFi} is higher than that on Q_{LF}.

5 Conclusion

The dead volume in the SMB plant is conceptualized as extra-column (e.g., bed-head and bed-tail) and bed-line dead

volumes and is responsible for up to 3 % of the bed volume. In the PX SMB configuration, the extract contamination due to bed-line dead volume is resolved by adding the flushing scheme, which increases the number of the SMB zone to 7 or 8. Numerous one dimensional SMB models taking dead volume and flushing application into account have been established. However, the geometry (length and diameter) of dead volume has been over-simplified and little attention has been paid to determining the axial dispersion inside dead volume.

This study investigated the effect of the dead volume geometry on concentration dynamics of a 7-zone PX SMB in the presence of axial dispersion, and demonstrated that a complex geometry of dead volume can be modeled into a simple geometry by using a geometric factor to have the same SMB simulation results. A fast and accurate solution tool for chromatography and SMB (FAST-Chrom/SMB) was used to calculate the 7-zone PX SMB model.

When the same axial dispersion coefficient is applied, a different geometry results in a different concentration profile inside dead volume, where a short and wide geometry shows a dispersive flow. The different concentration profiles lead to different simulation and optimization results. Since the complex geometry of dead volume is often simplified into a representative geometry in one dimensional SMB modeling, it is necessary to know how to convert the complex geometry into a simple one, keeping the same concentration dynamics. Applying the shape factor to the dispersion coefficient when the geometry changes, a quasi identical simulation result was successfully obtained in the 7-zone PX SMB. However, the application of the shape factor is limited to one-dimensional convection-diffusion equation for dead volume where a high level of complexity like distributors and internal piping is ignored and is assumed as a lumped axial dispersion. Optimal flushing flow rates were identified by parametric study, maximizing recovery within a desired purity.

Acknowledgements This research was supported by Basic Science Research Program through the National Research Foundation of Korea (NRF) funded by the Ministry of Education, Science and Technology (Grant number: 2011-0006827). The author also appreciates the editing contribution of Patrick Bresnahan.

References

Antos, D., Seidel-Morgenstern, A.: Application of gradients in the simulated moving bed process. Chem. Eng. Sci. **56**(23), 6667–6682 (2001)

Azevedo, D.C.S.: FEUP separation/reaction in simulated moving bed application to the production of industrial sugars. PhD dissertation, University of Porto, Portugal (2001)

Azevedo, D.C.S., Neves, S.B., Ravagnani, S.P., Cavalcante, C.L. Jr., Rodrigues, A.E.: The influence of dead zones on simulated moving bed units. In: Meunier, F. (ed.) Fundamentals of Adsorption, vol. 6, pp. 521–526. Elsevier, Amsterdam (1998)

Beste, Y.A., Lisso, M., Wozny, G., Arlt, W.: Optimization of simulated moving bed plants with low efficient stationary phases: separation of fructose and glucose. J. Chromatogr. A **868**(2), 169–188 (2000)

Bosma, J.C.: More efficient process chromatography. PhD dissertation, Rijksuniversiteit Groningen, Netherlands (2001)

Broughton, D.B., Gerhold, C.G.: Continuous sorption process employing fixed bed of sorbent and moving inlets and outlets. US Patent 2985589 (1961)

Dünnebier, G., Klatt, K.U.: Modelling and simulation of nonlinear chromatographic separation processes: a comparison of different modelling approaches. Chem. Eng. Sci. **55**(2), 373–380 (2000)

Fogler, H.S.: Elements of Chemical Reaction Engineering, 4th edn. Prentice Hall, New York (2005)

Frey, S.J.: Product recovery from simulated-moving-bed adsorption. US Patent 7208651 (2007)

Grosfils, V.: Modelling and parametric estimation of simulated moving bed chromatographic processes (SMB). PhD dissertation, Universite Libre De Bruxelles, Belgium (2009)

Grosfils, V., Hanus, R., Wouwer, A.V., Kinnaert, M.: Parametric uncertainties and influence of the dead volume representation in modelling simulated moving bed separation processes. J. Chromatogr. A **1217**(47), 7359–7371 (2010)

Jin, W., Wankat, P.C.: Thermal operation of four-zone simulated moving beds. Ind. Eng. Chem. Res. **46**, 7208–7220 (2007)

Juza, M., Mazzotti, M., Morbidelli, M.: Simulated moving-bed chromatography and its application to chirotechnology. Trends Biotechnol. **18**(3), 108–118 (2000)

Katsuo, S., Langel, C., Schanen, P., Mazzotti, M.: Extra-column dead volume in simulated moving bed separations: theory and experiments. J. Chromatogr. A **1216**(7), 1084–1093 (2009)

Kurup, A.S., Hidajat, K., Ray, A.K.: Optimal operation of an industrial-scale Parex process for the recovery of p-xylene from a mixture of C_8 aromatics. Ind. Eng. Chem. Res. **44**(15), 5703–5714 (2005)

Levenspiel, O.: Chemical Reaction Engineering. Wiley, New York (1999)

Lim, Y.-I., Bhatia, S.: Effect of dead volume on performance of simulated moving bed process. Adsorption **17**, 109–120 (2011)

Lim, Y.-I., Jorgensen, S.B.: A fast and accurate numerical method for solving simulated moving bed (SMB) chromatographic separation problems. Chem. Eng. Sci. **59**(10), 1931–1947 (2004)

Lim, Y.-I., Lee, J., Bhatia, S.K., Lim, Y.-S., Han, C.: Improvement of para-xylene SMB process performance on an industrial scale. Ind. Eng. Chem. Res. **49**(7), 3316–3327 (2010)

Migliorini, C., Mazzotti, M., Morbidelli, M.: Simulated moving-bed units with extra-column dead volume. AIChE J. **45**(7), 1411–1421 (1999)

Minceva, M., Rodrigues, A.E.: Modeling and simulation of a simulated moving bed for the separation of p-xylene. Ind. Eng. Chem. Res. **41**(14), 3454–3461 (2002)

Minceva, M., Rodrigues, A.E.: Influence of the transfer line dead volume on the performance of an industrial scale simulated moving bed for p-xylene sseparation. Sep. Sci. Technol. **38**(7), 1463–1497 (2003)

Minceva, M., Rodrigues, A.E.: Two-level optimization of an existing SMB for p-xylene separation. Comput. Chem. Eng. **29**(10), 2215–2228 (2005)

Minceva, M., Rodrigues, A.E.: Understanding and revamping of industrial scale SMB units for p-xylene separation. AIChE J. **53**(1), 138–149 (2007)

Mun, S., Xie, Y., Wang, N.-H.L.: Robust pinched-wave design of a size-exclusion simulated moving-bed process for insulin purification. Ind. Eng. Chem. Res. **42**(13), 3129–3143 (2003)

Nauman, E.B.: Chemical Reactor Design, Optimization, and Scaleup. McGraw-Hill, New York (2001)

Noe, R.J.L.: Raffinate line flush in simulated continuous moving bed adsorptive separation process. US Patent 5912395 (1999)

Pais, L.S., Loureiro, J.M., Rodrigues, A.E.: Modeling strategies for enantiomers separation by SMB chromatography. AIChE J. **44**(3), 561–569 (1998)

Sá Gomes, P., Lamia, N., Rodrigues, A.E.: Design of a gas phase simulated moving bed for propane/propylene separation. Chem. Eng. Sci. **64**(6), 1336–1357 (2009)

Seidel-Morgenstern, A., Keßler, L.C., Kaspereit, M.: New developments in simulated moving bed chromatography. Chem. Eng. Technol. **31**(6), 826–837 (2008)

Stern, D.L., Brown, S.H., Beck, J.S.: Isomerization and transalkylation of alkylaromatics. In: Ertl, G., Knozinger, H., Schuth, F., Weitkamp, J. (eds.) Handbook of Heterogeneous Catalysis. Wiley-VCH, New York (2008)

UOP: Aromatics complex (para-xylene). http://www.uop.com/ (2010). Accessed October 2010

Wei, C.N.: Multiple grade flush adsorption separation process. US Patent 5750820 (1998)

Wooley, R., Ma, Z., Wang, N.H.L.: A nine-zone simulating moving bed for the recovery of glucose and xylose from biomass hydrolyzate. Ind. Eng. Chem. Res. **37**(9), 3699–3709 (1998)

Zabka, M., Minceva, M., Gomes, P.S., Rodrigues, A.E.: Chiral separation of R,S-α-tetralol by simulated moving bed. Sep. Sci. Technol. **43**(4), 727–765 (2008)